

# DISTINGUISH Workflow: A New Paradigm of Dynamic Well Placement Using Generative Machine Learning

Sergey Alyaev<sup>1\*</sup>, Kristian Fossum<sup>1</sup>, Hibat Errahmen Djecta<sup>1,2</sup>,  
Jan Tveranger<sup>1</sup>, Ahmed H. Elsheikh<sup>3</sup>

<sup>1</sup>NORCE Norwegian Research Centre AS, Bergen, Norway.

<sup>2</sup>University of Stavanger, Stavanger, Norway.

<sup>3</sup>Heriot-Watt University, Edinburgh, United Kingdom.

\*Corresponding author(s). E-mail(s): [saly@norce-research.no](mailto:saly@norce-research.no);

## Abstract

The real-time process of directional changes while drilling, known as geosteering, is crucial for hydrocarbon extraction and emerging directional drilling applications such as geothermal energy, civil infrastructure, and CO<sub>2</sub> storage. The geo-energy industry seeks an automatic geosteering workflow that continually updates the subsurface uncertainties and captures the latest geological understanding given the most recent observations in real-time.

We propose “DISTINGUISH”: a real-time, AI-driven workflow designed to transform geosteering by integrating Generative Adversarial Networks (GANs) for geological parameterization, ensemble methods for model updating, and global discrete dynamic programming (DDP) optimization for complex decision-making during directional drilling operations. The DISTINGUISH framework relies on offline training of a GAN model to reproduce relevant geology realizations and a Forward Neural Network (FNN) to model Logging-While-Drilling (LWD) tools’ response for a given geomodel.

This paper introduces a first-of-its-kind workflow that progressively reduces GAN-geomodel uncertainty around and ahead of the drilling bit and adjusts the well plan accordingly. The workflow automatically integrates real-time LWD data with a DDP-based decision support system, enhancing predictive models of geology ahead of drilling and leading to better steering decisions. We present a simple yet representative benchmark case and document the performance target achieved by the DISTINGUISH workflow prototype. This benchmark will be a foundation for future methodological advancements and workflow refinements.

# 1 Introduction

Dynamic real-time adjustment of well trajectory, or geosteering, is established in hydrocarbon drilling operations to maximize efficiency and safety [19]. Traditionally, geosteering has depended heavily on the manual interpretation of real-time Logging-While-Drilling (LWD) data, a challenging task under the pressure of rapid drilling operations and complex geological uncertainties [11, 36]. The application of geosteering extends beyond hydrocarbon wells to geothermal [39], civil infrastructure, and emerging domains like CO2 storage [28], further underscoring its importance.

Current methodologies developed for well-planning incorporate Ensemble-based Closed-Loop Reservoir Management (EnCLRM), which has set a new standard for probabilistic estimate of subsurface uncertainties [18, 37, 1] and informed decision support [17]. Despite its effectiveness, implementing EnCLRM in real-time scenarios is limited by the computational demands of its complex modeling sequences. Within these sequences, the geomodeling that involves depth conversion, structural modeling, faults, facies modeling on a grid, and property modeling [37] is among the hardest to automate and adapt for real-time operations.

Recent technological innovations have introduced generative machine learning, including variational auto-encoders [8], Generative Adversarial Networks (GAN) [9], and, lately, latent diffusion models [27, 13] as powerful tools for geomodeling. We will refer to them as GANs despite meaning a larger class of models. These models, capable of rapidly producing realistic geomodel realizations from a reduced set of parameters, provide a promising approach to overcoming traditional limitations. Alyaev et al. [7] and Fossum et al. [15] demonstrated that GANs combined with ensemble methods enable quick updates to geological models in response to acquired drilling data. Thus, GAN-based workflows can potentially transform geosteering into a more quantifiable and precise process.

While in field operations, decisions remain the responsibility of a geosteering team [19, 36], academic studies have advanced decision optimization methods to enhance efficiency and consistency. Initial approaches, such as greedy optimization, were employed by Chen et al. [10] and Kullawan et al. [24], focusing on immediate gains at each decision stage, but often resulted in sub-optimal outcomes due to the lack of future consideration [25]. Pavlov et al. [32] expanded on greedy optimization by integrating real-time formation evaluation data and differential evolution algorithms to optimize drilling trajectories, showing improvements over traditional methods.

To address the limitations of greedy optimization, Kullawan et al. [25] introduced Approximate Dynamic Programming (ADP) for geosteering, which incorporates future decisions and learning for proactive, globally optimized decision-making, superseding the greedy approaches in many scenarios. Despite its effectiveness, ADP's high computational demands and scenario-specific design pose challenges for real-time applications. A simplified version of ADP, termed 'naive-optimistic' [3], was proposed to enhance adaptability, albeit with a loss of proven optimality [4]. Nevertheless, it outperformed most experts in a synthetic experiment [5]. Outside of geosteering, for sequential well location selection to avoid subsurface caves, Kanfar et al. [22] explored the application of GANs combined with the Fast Informed Bound (FIB) algorithm, which utilizes elements of ADP to compute upper bounds on the value function.

Recently, reinforcement learning (RL) has emerged as a promising alternative to ADP methods, offering flexibility and computational efficiency once trained. RL trains an agent through iterative learning from environmental interactions, thereby developing optimal decision-making strategies suited for real-time scenarios. Kristoffersen et al. [23] presented the use of the 'NEAT' evolutionary RL algorithm to incorporate the effects of geosteering during well planning, demonstrating another aspect of decision optimization. Muhammad et al. [29] demonstrated that Deep Q-Network (DQN) algorithm achieves comparable and sometimes better results than ADP in geosteering optimization. Muhammad et al. [31] combined DQN with particle filter, achieving a performance that ranked above the top quartile participants in the close-to-realistic ROII Geosteering World Cup 2021, unconventional stage [30].

This paper introduces the "DISTINGUISH" workflow, a complete geosteering approach that integrates an updatable ensemble of GANs within a probabilistic framework for dynamic well placement. The workflow is modular, allowing for the combination of different generative geomodels and various measurements, with diverse data assimilation and decision support algorithms, making it easily adaptable to other geosteering scenarios. Our initial implementation utilizes real-time ultra-deep electromagnetic (UDAR) data and a robust Decision Support System (DSS), combining the Ensemble Kalman filter (EnKF), GAN-based geomodels, and the adapted 'naive-optimistic' ADP. The DISTINGUISH workflow enhances the precision of real-time subsurface modeling and decision-making by automating geosteering through a closed loop of sequential decisions and data acquisition. It moves towards an 'autopilot' capability for complex geosteering challenges.

## 2 Method

The DISTINGUISH workflow consists of two parts: the offline (pre-job) phase and the online phase. The online phase relies on selecting a geological prior and is enabled by offline training: we train a GAN model to reproduce relevant geology realizations and a Forward Neural Network (FNN) to model LWD tools' response for a given geomodel. The offline phase is identical to our previous study and is described thoroughly in Alyaev et al. [5].

Figure 1(a) depicts the online phase of the workflow. It begins with the initialization of an ensemble of model vectors, encoding various geological and petrophysical properties necessary for subsequent simulation and optimization tasks into a 60-dimensional multivariate normal distribution. The AI-driven sequence that maps the model vectors to these quantities of interest is central to the workflow; see Figure 1(b).

The mapping sequence, the same as introduced in Alyaev et al. [7], Fossum et al. [15], starts with the model vectors undergoing a GAN-generator mapping to realizations of facies-and-properties "images," providing simplified local geomodel representations. Subsequently, these images (which we call GAN-geomodels) are passed as input to the FNN model which acts as a fast proxy for simulating the LWD measurements. Its output is an ensemble of expected well-log responses based on the geomodels.

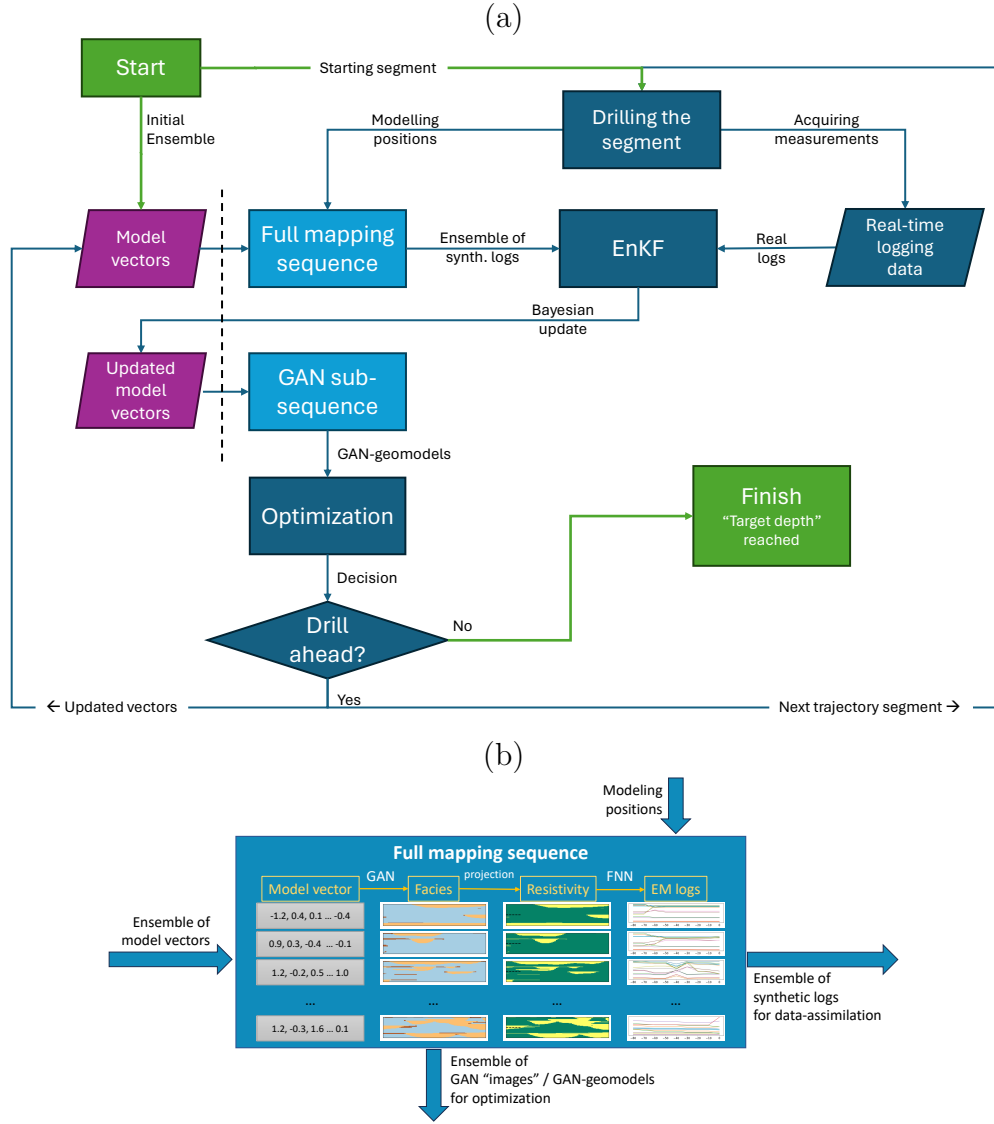


**Fig. 1** Overview of the DISTINGUISH workflow: (a) the online phase, and (b) a detailed schematic of the "full mapping sequence" highlighting its inputs and outputs.

Meanwhile, real well logs are acquired during the drilling process in the same positions. These logs offer actual measurements of the subsurface properties and are crucial for reducing uncertainty in the model predictions.

The EnKF computes the statistical misfit between the ensemble of predicted measurements and the actual well logs, see Figure 1(a). This misfit forms the basis for a Bayesian update of the model vectors, refining them to better match the observed data.

The updated model vectors are again converted into GAN-geomodels using the GAN sub-sequence. The GAN-geomodel ensemble now incorporates the latest subsurface information with reduced uncertainty in predicted geology ahead of the drill bit.

The GAN-geomodel ensemble is input into the decision support system, which combines optimization and visual methods to assist in making informed decisions about the remaining drilling trajectory. A dynamic programming optimization method recommends the drilling-trajectory next segment or stopping to maximize the operational objective. At the same time, the visualization provides explainability and helps the operational team understand the subsurface structure, the uncertainties, and the DSS recommendations.

The process is sequential, continuously updating and refining the model vectors and the corresponding GAN-geomodels as new real-time data becomes available during drilling. At each step, the team supported by the DSS makes a decision on whether to continue drilling based on the reached and potential targets. If the drilling continues, the workflow loops back, acquiring more real-time logging data and updating the models accordingly. The workflow concludes when the "target depth" is reached, resulting in an optimized trajectory and accurate geological model around the drilled well.

## 2.1 Full mapping sequence

The full mapping sequence of the DISTINGUISH workflow (Figure 1(b)) consists of several steps enabled by offline training of several neural networks (NNs):

- A GAN generator maps model vectors to facies images;
- A petrophysical model maps images to resistivity profiles;
- An FNN maps resistivities to EM logs along the drilled trajectory.

The first stage begins with model vectors, which are 60-dimensional in our case. The vector parametrization is learned during the adversarial training of the GAN, which consists of two NNs: a generator and a discriminator, both with deep convolutional architecture. During training, the generator converts vectors selected randomly from a multivariate normal distribution into synthetic facies images, trying to resemble real geological models from the training data. Simultaneously, the discriminator learns to distinguish between real and generated images. In this study, the output images have a fixed size of 64x64 cells with three channels, each corresponding to a probability of each facies (channel, crevasse, and floodplain shale). This offline training process ensures that the generated facies images are geologically plausible, the corresponding model vectors are distributed as multivariate normal Gaussian, and the mapping between them maps small changes of vectors into small changes in resulting geologies. The full training details are provided in Alyaev et al. [7], and the 3D fluvial geomodel dataset generated using geological software is described in the Appendix.

Following the GAN-generated facies images (GAN-geomodels for short), the next stage involves projecting these images to resistivity models. In this study, same as Alyaev et al. [7], we employ a petrophysical model that maps each facies to a constant resistivity value, specifically 4.0 ohm-m for floodplain shale, 171.0 ohm-m for

oil-saturated channel sand, and 55.0 ohm-m for partially saturated crevasse splay sand. This projection captures the electrical properties of the subsurface formations, translating the geological features into resistivity models that can be used for further analysis.

In the final stage, these resistivity models are used to generate synthetic EM-log responses along the trajectory. For each logging position (one per vertical column), we compute the distances to boundaries between facies from the virtual location of the measuring tool (modeling position, see Figure 1(b)). The vertical distances and the layer resistivities are fed into a pre-trained FNN that produces electromagnetic (EM) logs. This study uses the pre-trained forward model FNN described in Alyaev et al. [6] that reproduces the full suite of extra-deep azimuthal resistivity (EDAR) EM logs. In practice, the FNN must be trained for the relevant geological setting [35]. The EDAR FNN model has up-down sensitivity for up to six boundaries, potentially covering the full GAN-geomodel thickness of 32 meters from any measurement position. Thus, EDAR EM logs contain information about the subsurface’s electrical properties, which is essential for updating the geomodel and accurate geosteering.

The mapping sequence serves two key purposes: providing geological predictions around and ahead of the bit and transforming these predictions into relevant measurements. The modularity of the workflow allows for flexible adjustments in both areas. The mapping to local geological models - such as facies images - captures critical subsurface configurations and uncertainties, which are required for optimization. At the same time, the mapping to relevant real-time LWD measurements - such as EM logs - informs the model updates under uncertainty. This dual-purpose structure ensures that the workflow remains adaptable. It allows each component to evolve independently as new data or complexities are introduced, making it an effective tool for geosteering and real-time decision-making.

## 2.2 EnKF for data assimilation and model updates

The full mapping sequence, as described above, maps a Gaussian model vector into a synthetic EM-log. Given measurements of real-time logging data, one can then update the model vectors and implicitly the GAN-geomodels by solving the statistical inverse problem. Encouraged by the results obtained in [15], we employ ensemble-based data assimilation to solve the inverse problem. Adapting to the sequential nature of the DSS, we choose the EnKF for data assimilation already demonstrated for other geosteering tasks in Chen et al. [10] and Alyaev et al. [4].

The EnKF updates the system states sequentially using Bayesian principles each time new observations are received. In a geosteering operation, LWD measurements are acquired and transmitted to the surface as the well is drilled, making the EnKF’s sequential nature well-suited for this problem. In this context, the system state corresponds to the poorly known earth model, and updates of the system state correspond to solving the inverse problem [20].

Considering the model and observations as stochastic variables, we use Bayes’ theorem to solve for the conditional distribution up to a normalizing constant

$$p(m|d) \propto p(d|m)p(m). \quad (1)$$

Here,  $p(d|m)$  is the likelihood and  $p(m)$  is the prior distribution of the model. In the EnKF, Bayes' theorem is used recursively to update the model at each observation point by using the last posterior model as the current prior  $p(m_i) = p(m_{i-1}|d_{i-1})$ . In the following, we will omit the time index,  $i$ , and only focus on updates at a single measurement point.

Assuming that all variables have Gaussian distributions and that there is a linear relationship between the earth model and the EM-response, one can derive an analytical solution for the mean and covariance of the conditional distribution [21]. Approximating all instances of covariance and mean by Monte-Carlo estimates results in the ensemble update equation, see, e.g. [14]

$$M^a = M^p + C_{M,g(M)} (C_{g(M)} + C_d)^{-1} (D - g(M^p) + E). \quad (2)$$

Here,  $M$  denotes the ensemble matrix where each column is a realization of the earth model:  $M^p$  is the prior ensemble for a given step;  $M^a$  is the ensemble "analysis" matrix, conditioned to the new measurements. The shorthand  $g(M)$  denotes that the map from the model to synthetic EM-log has been applied to all columns (ensemble members) of  $M$ ,  $D$  is an ensemble matrix where each column is a copy of the current observation, and  $E$  is an ensemble matrix of measurement perturbations where each column ( $\epsilon_j$ ) is a realization of the Gaussian measurement error  $\epsilon_j \propto N(0, C_d)$ .  $C_d$  denotes the covariance matrix for the current measurements,  $C_{M,g(M)}$  denotes the Monte-Carlo estimate of the cross-covariance between the model and the predicted data, and  $C_{g(M)}$  denotes the Monte-Carlo estimate of the auto-covariance matrix for the predicted data.

The updated "analysis" ensemble of models,  $M^a$ , from the EnKF is the input to the optimization.

### 2.3 Optimization with approximate dynamic programming for decisions

The DISTINGUISH workflow incorporates an optimization step using 'naive-optimistic' ADP to optimize the remaining drilling trajectory based on updated GAN-geomodels. This method effectively navigates the high-dimensional space of possible trajectories, identifying the path that maximizes the operational objective by balancing geological target zones and operational constraints.

For each realization of GAN-geomodel in the "analysis" ensemble, our ADP method constructs a reward matrix  $R$  that quantifies the geological and operational desirability of drilling various segments. Each entry  $R_{i,j}(m)$  in this matrix represents the potential reward of steering the drill bit from point  $i$  to point  $j$ , given a realization of GAN-geomodel  $m$ . The goal is to find a sequential path  $\pi_k^*(m)$  among the potential paths  $\pi_k$  (starting from point  $k$ ) that maximizes the cumulative reward:

$$\pi_k^*(m) = \arg \max_{\pi_k} \sum_{(i,j) \in \pi_k} R_{i,j}(m). \quad (3)$$

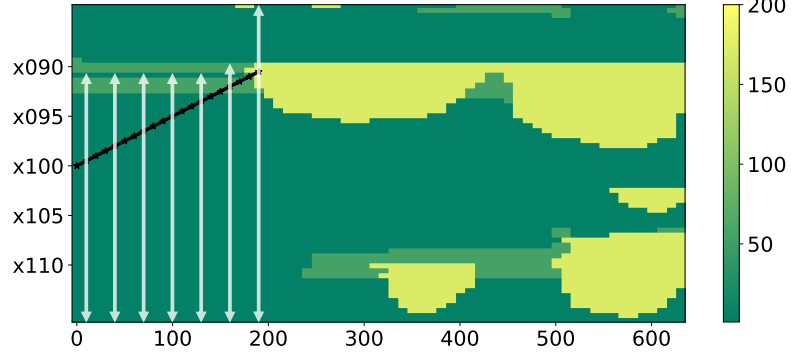


**Fig. 2** Resistivity of the synthetic truth (in Ohm-m). The line shows a possible well trajectory with stars in the measurement locations; the arrows show the tool sensitivity of up to three boundaries in an up or down direction. The measurement error is set to 10% relative noise.

In our implementation, the  $(\pi_k^*(m))_k = (l, m)$  are matrices of the regular positions in the geomodel grid  $(l, m)$ . These matrices are computed efficiently using dynamic programming principles [12] with a single pass through each entry in  $R_{i,j}(m)$ .

The tracing of the optimal path  $\pi$  starts from the kickoff point of the lateral reservoir section in which geosteering occurs. In this synthetic study, we start from the center of the leftmost column in the local GAN-geomodel.

At each step (starting from point  $k$ ), the ADP algorithm selects the single next decision  $\pi_k^{*1}(M^a)$  an admissible segment or stopping based on the maximum average expected reward:

$$\pi_k^{*1}(M^a) = \arg \max_{j, (k,j) \in \pi} \left( \frac{1}{N_e} \sum_{n \in N_e} [R_{k,j}(m_n) + \pi_j^*(m_n)] \right). \quad (4)$$

Since the ensemble of GAN-geomodels is updated after drilling each segment, the matrices  $\pi_j^*(m_n)$  need to be recomputed against new ensemble members. The repeated computation of these matrices is the practical reason for the 'naive-optimistic' simplification introduced in Alyaev et al. [2] and further analyzed in Alyaev et al. [4]. That is, we only perform the robust optimization accounting for uncertainties for the single next step, not taking the uncertainties along the entire trajectory into account.

The updating and optimization process continues until the target depth is reached or further drilling is unprofitable, ensuring that each step maximizes the immediate reward while accounting for the possible future gain. By combining AI-driven geomodeling with advanced optimization techniques, the DISTINGUISH workflow establishes a comprehensive framework for geosteering, enhancing the efficiency, reproducibility, and robustness of drilling decisions.



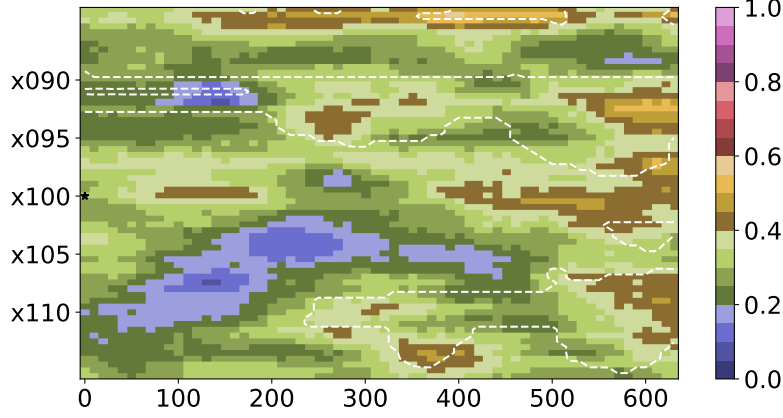


**Fig. 3** The prior model at the start of the operation with a star indicating the kick-off drilling position. The prior indicates approximately 40% probability of a sand body in the horizontal direction ahead of the bit. The image shows the probability of sand (either channel or crevasse) for every point based on the ensemble average. The white outline indicates the synthetic truth unknown to the DSS.

## 3 Results

As the initial synthetic benchmark for the DISTINGUISH workflow, we use the same synthetic truth as in Alyaev et al. [7], see Figure 2. The drilling starts in the middle of the GAN-geomodel.

### 3.1 Prior

The prior consists of 250 model vectors sampled from the same distribution as in Alyaev et al. [7]. At the start of drilling, it translates to an ensemble of GAN-geomodels with a large uncertainty in facies distribution, see Figure 3. The drilling starts horizontally in a floodplain shale indicated by the star in Figure 3, but the prior indicates an approximately 40% probability of a sand body in the horizontal direction ahead of the bit. Knowing the synthetic truth, based on intuition, we would like the DSS to reduce the uncertainty based on the measurements and redirect the well to the top channel sequence at a depth of x090, with the bottom channel sequence at a depth of x110 being a worse option.

### 3.2 Objective function and constraints

In a systematic decision analytics framework [26], assigning appropriate weights to different geological targets and estimating relative drilling costs are crucial for generating accurate reward matrices. The weights formalize the relative importance or desirability of drilling through different geological features. In this synthetic study, we use the following objective function:

$$R_{i,j} = -R_{i,j}^{\text{drill}} + R_j, \quad (5)$$

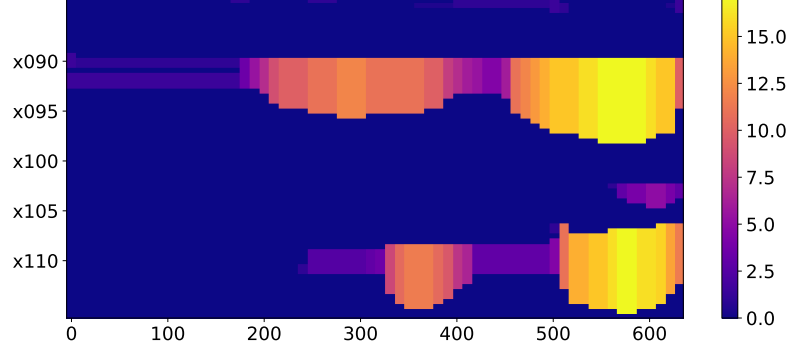


**Fig. 4** The weighted reward image for the synthetic truth, showing the relative value for reaching each of the cells. The cell values are computed according to Equation (6).

where  $R_{i,j}^{\text{drill}}$  is the drilling cost proportional to the drilled distance between point  $i$ , and  $j$  (set to 0.02 per meter drilled) and  $R_j$  is the reward for reaching the target at cell  $j$ . It is defined as:

$$R_j = \int_{k=j_0}^{j_l} w(f_k) dz, \quad (6)$$

where  $j_0$  and  $j_l$  are limits of continuous sand (crevasse or channel) in the vertical direction, and  $w(f_k)$  is the weight based on the facies type in each cell  $f_k$ . We define weights  $w(f_k)$  for key geological targets based on their facies type. For this study, the weights are defined as follows:

$$w(f_k) = \begin{cases} 1.0 & \text{if Oil-Saturated Sand Channel,} \\ 0.5 & \text{if Partially-Saturated Crevasse Splay Sand.} \end{cases} \quad (7)$$

The reward image composed of  $R_j$ -values for the synthetic true model, unknown to the DSS, is shown in Figure 4.

The ADP algorithm selects a path where each consecutive segment can go horizontally or diagonally, one cell up or down. The weighted reward images constructed for GAN-geomodel realizations updated at each step define the desirability of various paths. They inform the ADP algorithm's selection of the optimal drilling trajectory, taking into account both geological and operational factors.

### 3.3 Data-assimilation setup

We perform data assimilation by applying the analysis step (Equation (2)) from the Ensemble Smoother method implemented in the open-source PET library [16]. The sensitivity of our AI-based EM model closely resembles the EDAR tool [6]; it is illustrated for the true model in Figure 2.

We simulate a challenging scenario where we use 10% relative noise for all 13 components of the EM tool. This noise level is ten times higher than the noise considered

in the earlier GAN studies by Alyaev et al. [7] and Fossum et al. [15]. Thus, uncertainty quantification and robust decisions become essential for this new geosteering benchmark.

### 3.4 The benchmark results

Figure 5 illustrates the application of the DISTINGUISH DSS to the synthetic benchmark step by step. Here we try to justify the observed behaviour of the system.

The "landing" phase (Figure 5, column 1) starts from the data assimilation step one, which reveals the misfit of the initial prior (Figure 3) with the true model. After the data assimilation, the estimated probability of sand around the bit becomes low, indicating drilling in the shale.

The DSS optimization finds a suitable long-term target within each of the realizations. The resulting trajectory "fan" for Step 1 spans most of the model because the uncertainty is still high. Due to the GAN-geomodel structure, each of the realizations is geologically plausible, but the outline of the geo-bodies in less probable realization groups are averaged out in the figures. Note that we perturb the trajectory paths so that thick agglomerations of lines highlight the areas targeted across many realizations. At Step 1, the DSS recommendation is to build up the angle.

By Step 11, shown in the second row of Figure 5, as the EM tool nears the crevasse boundary, the assimilated data indicates a reservoir layer above the bit. However, the location and thickness are very uncertain and far from the synthetic truth (the white outline) due to large measurement errors. At Step 11, most of the long-term targets point at the preferred top reservoir sequence, and the DSS recommendation is to hold the angle and continue drilling up.

When the measurement tool reaches the sand at Step 16 (row 3, column 1 in Figure 5), we see a much clearer outline of the crevasse, which is also propagated along the channel sequence horizontally to geological continuity learned by the GAN. At the same time, erroneous sand 'artifacts' appear around 70m along x-axes, which are also produced by global correlations in our GAN model. These increased sand-probability regions become more or less pronounced during the next steps. This dramatically increases the probability of the sand extending horizontally throughout the model, mimicking the feature in the true model (white outline). This focuses the fan of trajectories on the x090-sand, leading to the decision to target it.

At Step 20 (row 4, column 1 in Figure 5), the well 'lands' in the first sand body in the x090 sequence. The EM LWD tool becomes sensitive to the roof of the sand channel and the boundaries above it. This reduces the probability of sand-layer sequence at the very top of the model, which seemed likely in the original prior. At this step, the decision is to drop and drill horizontally along the reached sand.

In column 2 of Figure 5, we observe the recommended well trajectory as the DSS follows the x090 sand sequence. Simultaneously, the DISTINGUISH workflow maps the sand bodies despite the large noise in the EM logs.

At Step 31 (row 1, column 2 in Figure 5), the bit is nearing the floor of the x090 sand-body sequence to have the option to steer into the sands stacked under it. The increased possibility of reservoir exit results in the DSS recommendation to build up and continue in the current sand body.

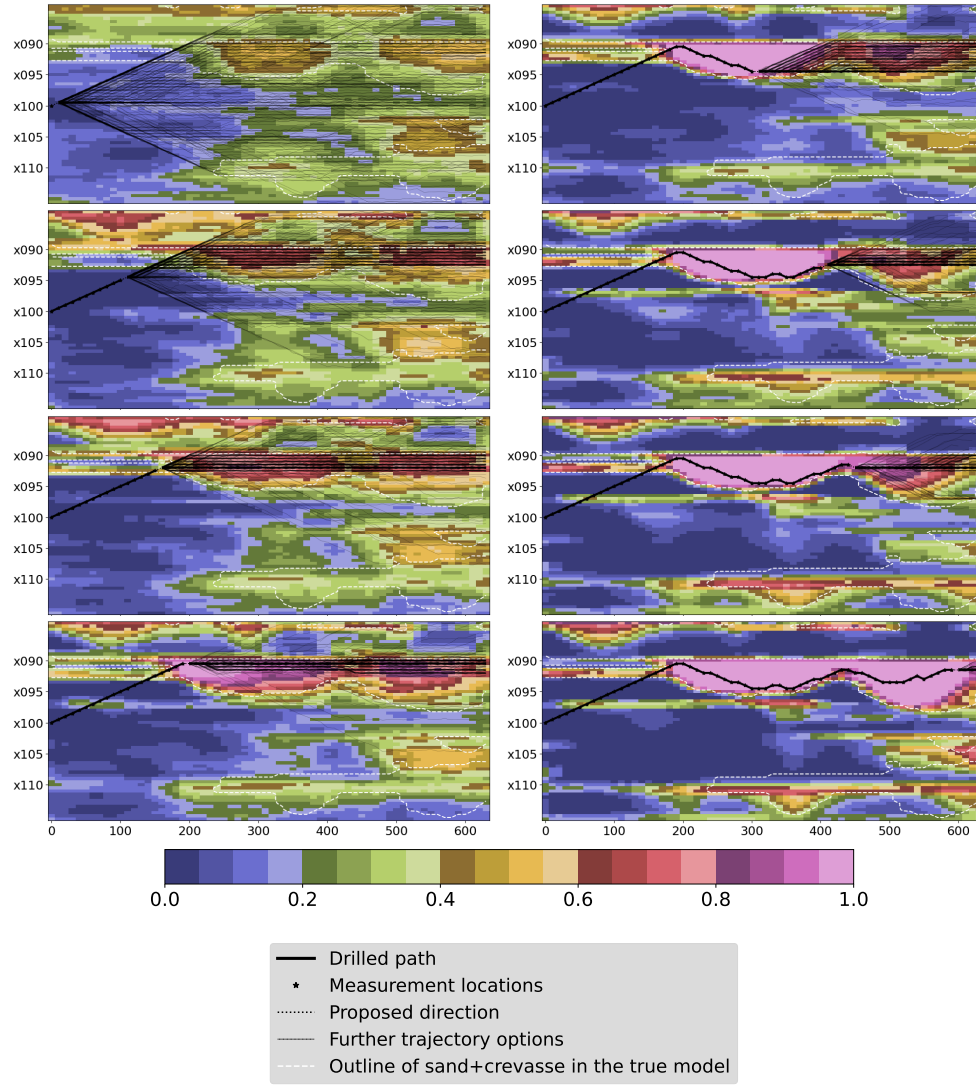


**Fig. 5** Illustration of the DISTINGUISH decision support system (DSS) applied to a synthetic scenario. This figure details the step-by-step decision recommendations provided by the DSS, indicated by the proposed-direction dashed line and advancing the bit in the next sub-figures. The "fan" of thin dashed trajectories, which start from the recommended decision, indicates path possibilities optimal for individual realizations in the ensemble. The trajectory paths in the fan are perturbed: thicker line agglomerates correspond to more trajectories targeting each area. The scenario begins with an initial geomodel uncertainty, which gradually decreases as EM measurements are collected during drilling (shown by stars). The background images show the probability of sand (channel or crevasse) after data assimilation at the current step. The outline of the true model is provided as a reference but is unknown to the DSS.

At Step 41 (row 2, column 2 in Figure 5), the bit reaches the crevasse splay between two large sand bodies in the sequence. The primary DSS target at this point is continuing in the x090 sand, but some realizations suggest a large stack of sand below it. The recommendation is to follow the former and to build up again.

At Step 45 (row 3, column 2 in Figure 5), we see how the new measurements reveal the last sand body in the sequence. The DSS recommends dropping and continuing in the middle of that sand body.

At Step 60 (row 4, column 2 in Figure 5), we see the final part of the benchmark operation. At this point, the decision is to continue along the sand. Simultaneously, the 60 assimilated log locations have significantly reduced the uncertainty and mapped out the drilled sand. Moreover, through the correlations learned by the GAN, the information also extends further away from the well, highlighting several channel sequences above and below. The sequence at the top of the model is well-identified. The channel stacking below the bit location at Step 60 is picked up, but the shapes cannot be correctly identified. Some of it extends erroneously to the left and along the x090 sequence. The reason is the global correlations and that the EnKF does not reuse the previous data, resulting in possible "forgetting" when the problem is not well-posed. On the other hand, the global correlations help identify the sand sequence at x110 almost invisible to the measurements.

In summary, the application of the DISTINGUISH DSS to the synthetic benchmark effectively demonstrates the system's capability to adaptively refine its drilling strategy based on real-time data assimilation and the GAN that learned geological knowledge during offline training. The iterative updates reduce uncertainty and enhance the accuracy of the geological interpretation, ultimately leading to more informed decision-making throughout the drilling process. Despite obvious room for further improvement, the results underscore the potential of an integrated system combining advanced AI techniques with data assimilation to optimize well placement and improve reservoir mapping.

## 4 Conclusions

We have introduced the DISTINGUISH workflow: a complete GAN-enabled decision support system for geosteering that progresses assisted geosteering towards high geological complexity, see Figure 6. The positive results observed in the presented synthetic benchmark case demonstrate the effectiveness of the DISTINGUISH workflow in refining drilling strategies through adaptive real-time data assimilation and AI-driven geological modeling. These results validate the potential of our approach to improve decision-making processes in geosteering operations.

We are committed to making the DISTINGUISH workflow open source, allowing the broader geoscience community to benefit from our advancements and contribute to further developments. By setting this benchmark, we aim to establish a foundation for the emerging field of real-time drilling supported by generative AI, which holds great promise for transforming traditional geoscience practices.

Despite these advancements, there is significant potential for future work, starting with addressing the artifacts observed in the model. Possible solutions are improved

# Assisted geosteering approaches in different scenarios

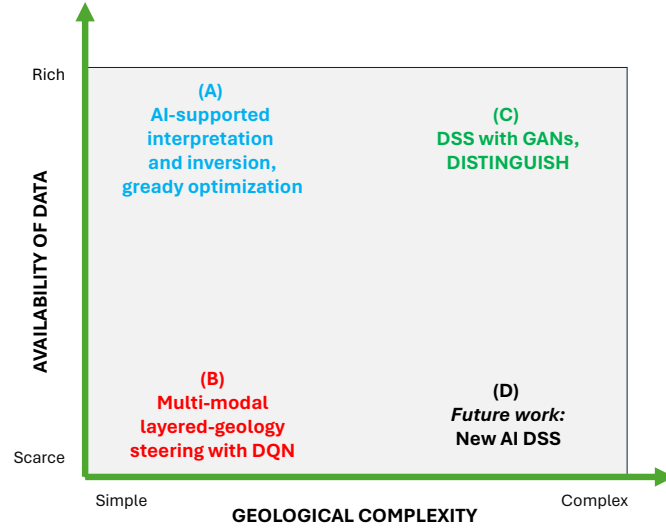


**Fig. 6** AI-assisted geosteering approaches depending on data availability and geological complexity. Examples (A): Rammay et al. [35], Pavlov et al. [32]; (B): Muhammad et al. [30, 31]; (C): this paper; (D): future developments of the DISTINGUISH workflow with improved planning and optimization algorithms based on RL.

data assimilation techniques and new generative AI methods for geomodeling. Adapting the workflow to field operations, including those with less data, will also require incorporating more realistic decision objectives and constraints and developing better decision-making methods. These efforts will enhance the robustness and applicability of the DISTINGUISH workflow, driving innovation in geosteering and geoscience in general.

## 5 Supporting Data and Code Availability

The code produced for this paper and running instructions are available in a public GitHub repository. You can access the repository at the following link: <https://github.com/geosteering-no/GAN-geosteering>. We plan further development and maturation of the repository.

## 6 CRediT author statement

**SA:** Conceptualization; Methodology; Software; Validation; Formal analysis; Writing - Original Draft; Writing - Review and Editing; Visualization; Supervision; Project administration; Funding acquisition. **KF:** Conceptualization; Methodology; Software; Validation; Formal analysis; Investigation; Writing - Original Draft; Visualization; Supervision. **HJ:** Software; Validation; Investigation; Writing - Original Draft; Visualization. **JT:** Conceptualization; Methodology; Data Curation; Writing - Original

Draft; Writing - Review and Editing; Visualization. **AE**: Conceptualization; Writing - Review and Editing.

## 7 Statement on AI-generated text

The authors used Open AI ChatGPT to improve draft paragraphs. The AI-generated text was carefully edited to reflect the authors' opinions and perceptions. Most of the text was also processed using Grammarly and its AI Paraphrase Tool to improve formulations and grammar. The authors take full ownership of the study's content and conclusions.

## 8 Acknowledgements

This work is part of the project DISTINGUISH: Decision support using neural networks to predict geological uncertainties when geosteering, funded by Aker BP, Equinor, and the Research Council of Norway (RCN PETROMAKS2 project no. 344236). We gratefully acknowledge Aspentech for providing an academic software license for Aspen RMS<sup>TM</sup> used for creating the geomodel dataset.

## References

- [1] Anahita Abadpour, Moyosore Adejare, Tatiana Chugunova, Helene Mathieu, and Norman Haller. Integrated geo-modeling and ensemble history matching of complex fractured carbonate and deep offshore turbidite fields, generation of several geologically coherent solutions using ensemble methods. In *Abu Dhabi International Petroleum Exhibition and Conference*, page D041S094R001. SPE, 2018. doi: 10.2118/193156-MS. URL <https://doi.org/10.2118/193156-MS>.
- [2] Sergey Alyaev, Reidar Brumer Bratvold, Xiaodong Luo, Erich Suter, and Erlend H Vefring. An interactive decision support system for geosteering operations. In *SPE Norway Subsurface Conference*, page D011S004R001. SPE, 2018. doi: 10.2118/191337-MS. URL <https://doi.org/10.2118/191337-MS>.
- [3] Sergey Alyaev, Aojie Hong, and Reidar B Bratvold. Are you myopic, naïve or farsighted about your geosteering decisions? In *Second EAGE/SPE Geosteering and Well Placement Workshop*, volume 2018, pages 1–5. European Association of Geoscientists & Engineers, 2018. doi: 10.2118/195067-MS. URL <https://doi.org/10.2118/195067-MS>.
- [4] Sergey Alyaev, Erich Suter, Reidar Brumer Bratvold, Aojie Hong, Xiaodong Luo, and Kristian Fossum. A decision support system for multi-target geosteering. *Journal of Petroleum Science and Engineering*, 183:106381, 2019. doi: 10.1016/j.petrol.2019.106381. URL <https://doi.org/10.1016/j.petrol.2019.106381>.
- [5] Sergey Alyaev, Sofija Ivanova, Andrew Holsaeter, Reidar Brumer Bratvold, and Morten Bendiksen. An interactive sequential-decision benchmark from geosteering. *Applied Computing and Geosciences*, 12:100072, 2021. doi: 10.1016/j.acgeo.2020.100072. URL <https://doi.org/10.1016/j.acgeo.2020.100072>.
- [6] Sergey Alyaev, Mostafa Shahriari, David Pardo, Ángel Javier Omella, David Selvåg Larsen, Nazanin Jahani, and Erich Suter. Modeling extra-deep



- electromagnetic logs using a deep neural network. *Geophysics*, 86(3):E269–E281, 2021. doi: 10.1190/geo2020-0200.1. URL <https://doi.org/10.1190/geo2020-0200.1>.
- [7] Sergey Alyaev, Jan Tveranger, Kristian Fossum, and Ahmed H Elsheikh. Probabilistic forecasting for geosteering in fluvial successions using a generative adversarial network. *First Break*, 39(7):45–50, 2021. doi: 10.3997/1365-2397.fb2021075. URL <https://doi.org/10.3997/1365-2397.fb2021075>.
  - [8] Smith WA Canchumuni, Alexandre A Emerick, and Marco Aurélio C Pacheco. Towards a robust parameterization for conditioning facies models using deep variational autoencoders and ensemble smoother. *Computers & Geosciences*, 128: 87–102, 2019. doi: 10.1016/j.cageo.2019.04.012. URL <https://doi.org/10.1016/j.cageo.2019.04.012>.
  - [9] Shing Chan and Ahmed H Elsheikh. Parametrization and generation of geological models with generative adversarial networks. *arXiv preprint arXiv:1708.01810*, 2017. doi: 10.48550/arXiv.1708.01810. URL <https://doi.org/10.48550/arXiv.1708.01810>.
  - [10] Yan Chen, Rolf J Lorentzen, and Erlend H Vefring. Optimization of well trajectory under uncertainty for proactive geosteering. *SPE Journal*, 20(02):368–383, 2015. doi: 10.2118/172497-PA. URL <https://doi.org/10.2118/172497-PA>.
  - [11] Yasaman Cheraghi, Sergey Alyaev, Aojie Hong, Igor Kuvaev, Stephen Clark, Andrei Zhuravlev, and Reidar Brumer Bratvold. What can we learn after 10,000 geosteering decisions? In *SPE/AAPG/SEG Unconventional Resources Technology Conference*, page D021S022R002. URTEC, 2022. doi: 10.15530/urtec-2022-3777325. URL <https://doi.org/10.15530/urtec-2022-3777325>.
  - [12] Thomas H Cormen, Charles E Leiserson, Ronald L Rivest, and Clifford Stein. *Introduction to algorithms*. MIT press, 2022. URL <https://mitpress.mit.edu/9780262046305/introduction-to-algorithms/>.
  - [13] Guido Di Federico and Louis J Durlafsky. Latent diffusion models for parameterization and data assimilation of facies-based geomodels. *arXiv preprint arXiv:2406.14815*, 2024. doi: 10.48550/arXiv.2406.14815. URL <https://doi.org/10.48550/arXiv.2406.14815>.
  - [14] Geir Evensen, Femke C. Vossepoel, and Peter Jan van Leeuwen. *Data Assimilation Fundamentals*. Springer Textbooks in Earth Sciences, Geography and Environment. Springer International Publishing, 2022. ISBN 978-3-030-96708-6. doi: 10.1007/978-3-030-96709-3. URL <https://doi.org/10.1007/978-3-030-96709-3>.
  - [15] Kristian Fossum, Sergey Alyaev, Jan Tveranger, and Ahmed H Elsheikh. Verification of a real-time ensemble-based method for updating earth model based on GAN. *Journal of Computational Science*, 65:101876, 2022. doi: 10.1016/j.jocs.2022.101876. URL <https://doi.org/10.1016/j.jocs.2022.101876>.
  - [16] Kristian Fossum, Sergey Alyaev, and Ahmed H Elsheikh. Ensemble history-matching workflow using interpretable SPADE-GAN geomodel. *First Break*, 42(2):57–63, 2024. doi: 10.3997/1365-2397.fb2024014. URL <https://doi.org/10.3997/1365-2397.fb2024014>.
  - [17] Remus Gabriel Hanea, Ole Petter Bjorlykke, Yastoor Hashmi, Tao Feng, and Rahul Mark Fonseca. Robust multi-objective field development optimization for



- the mariner asset. In *SPE Reservoir Simulation Conference*, page D021S013R005. SPE, 2019. doi: 10.2118/193914-MS. URL <https://doi.org/10.2118/193914-MS>.
- [18] RG Hanea, RM Fonseca, C Pettan, MO Iwajomo, K Skjerve, L Hustoft, AG Chitu, and F Wilschut. Decision maturation using ensemble based robust optimization for field development planning. In *ECMOR XV-15th European Conference on the Mathematics of Oil Recovery*, pages cp–494. European Association of Geoscientists & Engineers, 2016. doi: 10.3997/2214-4609.201601774. URL <https://doi.org/10.3997/2214-4609.201601774>.
- [19] Kristine Hermanrud, Frank Antonsen, Maria Emilia Teixeira De Oliveira, Steen Agerlin Petersen, and Monica Constable. Future geosteering and well placement solutions from an operator perspective. In *SPE Annual Caspian Technical Conference*, page D013S003R003. SPE, 2019. doi: 10.2118/198377-MS. URL <https://doi.org/10.2118/198377-MS>.
- [20] Marco a Iglesias, Kody J H Law, and Andrew M. Stuart. Ensemble Kalman methods for inverse problems. *Inverse Problems*, 29(4):045001, apr 2013. ISSN 0266-5611. doi: 10.1088/0266-5611/29/4/045001. URL <https://doi.org/10.1088/0266-5611/29/4/045001>.
- [21] Andrew H. Jazwinski. *Stochastic Processes and Filtering Theory*. Academic Press, New York, 1970. ISBN 9780123815507.
- [22] Rayan Kanfar, Lama El Halabi, Tyler Hall, and Tapan Mukerji. Well placement optimization for avoiding caves using GANs and POMDPs. In *International Petroleum Technology Conference*. IPTC, 2024. doi: 10.2523/IPTC-24209-MS. URL <https://doi.org/10.2523/IPTC-24209-MS>.
- [23] Brage S Kristoffersen, Mathias C Bellout, Thiago L Silva, and Carl F Berg. An automatic well planner for complex well trajectories. *Mathematical Geosciences*, 53(8):1881–1905, 2021.
- [24] K Kullawan, RB Bratvold, and JE Bickel. Value creation with multi-criteria decision making in geosteering operations. *International Journal of Petroleum Technology*, 3(1):15–31, 2016. doi: 10.1016/j.petrol.2015.10.002. URL <https://doi.org/10.1016/j.petrol.2015.10.002>.
- [25] K Kullawan, RB Bratvold, and JE Bickel. Sequential geosteering decisions for optimization of real-time well placement. *Journal of Petroleum Science and Engineering*, 165:90–104, 2018. doi: 10.1016/j.petrol.2018.10.002. URL <https://doi.org/10.1016/j.petrol.2018.10.002>.
- [26] Kanokwan Kullawan, Reidar Bratvold, and JE E Bickel. A decision analytic approach to geosteering operations. *SPE Drilling & Completion*, 29(01):36–46, 2014. doi: 10.2118/163494-PA. URL <https://doi.org/10.2118/163494-PA>.
- [27] Daesoo Lee, Oscar Ovanger, Jo Eidsvik, Erlend Aune, Jacob Skauvold, and Ragnar Hauge. Latent diffusion model for conditional reservoir facies generation. *arXiv preprint arXiv:2311.01968*, 2023. doi: 10.48550/arXiv.2311.01968. URL <https://doi.org/10.48550/arXiv.2311.01968>.
- [28] Fabio Marco Miotti, Jaijith Sreekantan, and Kara Meunier. Machine learning look-ahead application for geosteering with uncertainty estimation. In *Abu Dhabi International Petroleum Exhibition and Conference*, page D011S023R002. SPE, 2022. doi: 10.2118/208796-MS. URL <https://doi.org/10.2118/208796-MS>.

- [29] Ressi Bonti Muhammad, Sergey Alyaev, and Reidar Brumer Bratvold. Optimal sequential decision-making in geosteering: A reinforcement learning approach. *arXiv preprint arXiv:2310.04772*, 2023. doi: 10.48550/arXiv.2310.04772. URL <https://doi.org/10.48550/arXiv.2310.04772>.
- [30] Ressi Bonti Muhammad, Yasaman Cheraghi, Sergey Alyaev, Apoorv Srivastava, and Reidar Brumer Bratvold. Enhancing geosteering with AI: Integrating a decision-making robot into a cloud-based environment and benchmarking against human experts. In *SPE Norway Subsurface Conference*, page D011S002R008. SPE, 2024. doi: 10.2118/213976-MS. URL <https://doi.org/10.2118/213976-MS>.
- [31] Ressi Bonti Muhammad, Apoorv Srivastava, Sergey Alyaev, Reidar Brumer Bratvold, and Daniel M Tartakovsky. High-precision geosteering via reinforcement learning and particle filters. *arXiv preprint arXiv:2402.06377*, 2024. doi: 10.48550/arXiv.2402.06377. URL <https://doi.org/10.48550/arXiv.2402.06377>.
- [32] Maksimilian Pavlov, Georgy Peshkov, Klemens Katterbauer, and Abdallah Alshehri. Geosteering based on resistivity data and evolutionary optimization algorithm. *Applied Computing and Geosciences*, 22:100162, 2024. doi: 10.1016/j.acgeo.2023.100162. URL <https://doi.org/10.1016/j.acgeo.2023.100162>.
- [33] Matthew J Pranter and Nicholas K Sommer. Static connectivity of fluvial sandstones in a lower coastal-plain setting: An example from the upper cretaceous lower williams fork formation, piceance basin, colorado. *AAPG bulletin*, 95(6):899–923, 2011. doi: 10.1306/12131010096. URL <https://doi.org/10.1306/12131010096>.
- [34] Matthew J Pranter, Alicia C Hewlett, Rex D Cole, Huabing Wang, and James Gilman. Fluvial architecture and connectivity of the williams fork formation: use of outcrop analogues for stratigraphic characterization and reservoir modelling. *Geological Society, London, Special Publications*, 387(1):57–83, 2014. doi: 10.1144/SP387.2. URL <https://doi.org/10.1144/SP387.2>.
- [35] Muzammil Hussain Rammay, Sergey Alyaev, David Selvåg Larsen, Reidar Brumer Bratvold, and Craig Saint. Strategic geosteering workflow with uncertainty quantification and deep learning: Initial test on the goliath field data. *Submitted to Geophysics (arXiv preprint arXiv:2210.15548)*, 2024. doi: 10.48550/arXiv.2210.15548. URL <https://doi.org/10.48550/arXiv.2210.15548>.
- [36] Stephen Rassenfoss. A study suggests geosteers often are missing the target. *Journal of Petroleum Technology*, 74(12):24–29, 2022. doi: 10.2118/0622-0024-JPT. URL <https://doi.org/10.2118/0622-0024-JPT>.
- [37] JA Skjervheim, X Van Lanen, D Hulme, V Røine Stenerud, E Zachariassen, S Liu, J Hove, and G Evensen. Integrated workflow for consistent model building from depth conversion to flow simulation-north sea field case. In *74th EAGE Conference and Exhibition incorporating EUROPEC 2012*, pages cp–293. European Association of Geoscientists & Engineers, 2012. doi: 10.3997/2214-4609.20148712. URL <https://doi.org/10.3997/2214-4609.20148712>.
- [38] SM Trampush, EA Hajek, KM Straub, and EP Chamberlin. Identifying autogenic sedimentation in fluvial-deltaic stratigraphy: Evaluating the effect of outcrop-quality data on the compensation statistic. *Journal of Geophysical Research: Earth Surface*, 122(1):91–113, 2017. doi: 10.1002/2016JF004067. URL <https://doi.org/10.1002/2016JF004067>.

- [//doi.org/10.1002/2016JF004067](https://doi.org/10.1002/2016JF004067).
- [39] Pierre Ungemach, Miklos Antics, Davide Di Tommaso, and Filippo Casali. Real time geosteering integrated services. a key issue in maximizing geothermal exposure and minimizing drilling and completion risks. a paris basin case study. In *SPE/IADC Drilling Conference and Exhibition*, page D021S002R004. SPE, 2021. doi: 10.2118/204132-MS. URL <https://doi.org/10.2118/204132-MS>.

## 9 Appendix

### 9.1 Geological setting and the training dataset

The present study employs a training dataset of 2D sections extracted from a synthetic 3D geological model generated using standard industrial reservoir modeling software. The same geological model was employed by Alyaev et al. [7].

The model consists of an un-faulted, orthogonal grid measuring 4000m x 1000m x 200m (XYZ), with a resolution of 10m x 10m x 0.5m, yielding 16 million grid cells. The depth range of the model is set at 1800m to 2000m TVD. The depositional architecture in the model is based on geometric data from outcrops of the fluvial, low net/gross, lower Williams Fork Formation (Cretaceous Mesa Verde Group) at Coal Canyon, Colorado, USA Pranter and Sommer [33], Pranter et al. [34], Trampush et al. [38], comprising channel-, crevasse-splay-, and overbank/floodplain shaly facies, see Figure 7. In the model, the flow direction of the fluvial system is set to  $45 \pm 10$  degrees, with no trend functions constraining the spatial distribution of channels. For detailed parameter settings used in the facies model setup, see Alyaev et al. [7]. Petrophysical values used here are simplified and assumed constant for each facies; see Table 1. The table also shows a simple constant reward for drilling in each facies type roughly proportional to porosity.

Facies	Mean Porosity (%)	Oil Content	Resistivity (ohm-m)	Reward
Channel Sand	20	Oil-saturated	171.0	1.0
Crevasse Splay Sand	12	Partially	55.0	0.5
Floodplain Shale	2	No	4.0	0.0

**Table 1** Mean porosity, oil content, resistivity, and "per-pixel" reward  $C$  for different facies types.

The training dataset consists of 2D XZ-sections measuring 64 x 64 cells (i.e., 640m x 32m) sampled throughout the geo-model. The third dimension of the sampled sections represents a facies probability index.

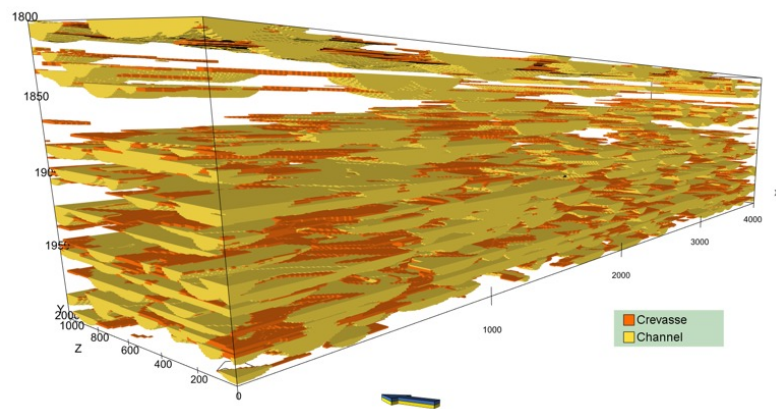


**Fig. 7** The facies structure of the synthetic 3D geoscientific model used for training. The background flood-plain shale facies are filtered out to highlight the distribution of channels and surrounding crevasse splays, underscoring the complexity of the model's 3D depositional architecture. Note 5x vertical exaggeration.